

Methods for improving the detection capabilities of environmental radioactivity measurements in the light of increased atmospheric radioactivity levels in 2020

Dorottya Jakab^{1,*}, Zsuzsa G. Endródi¹, Tamás Pázmándi¹ and Péter Zagyvai¹

¹Centre for Energy Research, Konkoly-Thege Miklós street 29-33. Budapest, 1121, Hungary

*Corresponding author's e-mail: jakab.dora@ek-cer.hu

Abstract. In 2020 several incidents occurred with certain environmental radiation protection implications. In April elevated radioactivity concentration of ^{137}Cs was measured across Europe as a consequence of the forest fire outbreaks in the Chernobyl exclusion zone. Furthermore, in early June the detection of various artificial radionuclides, such as ^{60}Co , ^{134}Cs , ^{137}Cs and ^{103}Ru , was reported by environmental monitoring stations of several Northern European countries. These events showed the continuous need for reliable radioactivity measurements to supply basic environmental radiological monitoring purposes. However, the increase in atmospheric radioactivity levels as a result of these events was generally low, which made it necessary to use highly sensitive measurement techniques or to endeavor improvement of detection capabilities of quantitative analysis. Methods are presented through concrete examples that achieved significant reduction of characteristic limits (decision threshold, detection limit) compared to detection capabilities of the environmental radiological monitoring system operating at the KFKI Campus in Budapest reachable under routine measurement conditions, by using the elements of the existing system, only by modifying the sampling and measurement procedures and the evaluation methods.

KEYWORDS: *Radioactivity measurements, Monitoring strategies, Artificial radionuclides, Decision threshold, Detection limit*

1 INTRODUCTION

In April 2020, forest wildfires broke out on in the Chernobyl exclusion zone which led to resuspension of ^{137}Cs into air from the contaminated areas around the damaged nuclear power plant. Consequently, ^{137}Cs activity concentrations in ground level air in Ukraine were significantly higher than their averages. Other countries also reported concentrations exceeding their usually observed ^{137}Cs levels (considered as “background”), justifying the movement of radioactive air masses towards to Western Europe. Although the activity concentrations measured outside of Ukraine were very low (typically below $10\ \mu\text{Bq}/\text{m}^3$), the incident led to a demonstrable increase in ^{137}Cs levels [1]. During June 2020, competent authorities of Scandinavian countries have reported the detection of various artificial radionuclides, such as ^{60}Co , ^{134}Cs , ^{137}Cs and ^{103}Ru in the atmosphere. Even though the activity concentrations were low again (in the order of a few tens of $\mu\text{Bq}/\text{m}^3$), so no radiological consequences were expected, the detection of a mixture of artificial radionuclides, most likely originated from irradiated material associated with nuclear reactors, had environmental radiation protection significance. Measurement results from other European countries did not indicate the presence of the aforementioned radionuclides, which was consistent with the atmospheric transport simulations that suggested very low-level contaminations of air masses [2]. These events emphasized the continuous need for reliable radioactivity measurements to supply basic environmental radiological monitoring purposes, such as providing data for supporting decision making on the necessity of protective actions. However, due to the generally low increase in atmospheric radioactivity levels as a consequence of these events, detectability required the use of highly sensitive measurement techniques or improvement of detection capabilities of quantitative analysis.

IRSN's atmospheric transport model calculations indicated that the contaminated air masses arose due to the fire outbreaks in Chernobyl reached Budapest, Hungary with maximum expected ^{137}Cs activity concentration of $10\text{-}20\ \mu\text{Bq}/\text{m}^3$ [1]. The estimated contamination of air masses, that probably reached Hungary around June 2020 from the direction of Scandinavia, were several order of magnitude lower (about $0.01\ \mu\text{Bq}/\text{m}^3$ [2]). The former levels correspond to the detection capabilities of the environmental radiological monitoring system operating at the KFKI Campus (located in Budapest; $47^\circ 29' 20.89''\text{N}$, $18^\circ 57' 13.44''\text{E}$) under routine measurement conditions. In order to be able to monitor such low activity concentrations, it was required to examine possibilities to improve the detection capabilities. In this paper, the methods used for the improvement of detection capabilities of environmental radioactivity measurements will be presented, with which significant reduction of characteristic limits (decision threshold, detection limit) was achieved by using the elements of the existing system only by modifying the sampling and measurement procedures and the evaluation methods. These approaches were

investigated with considering the aspects of practical applicability and data supply obligations to be met (e.g. the necessity for accurate but rapid data provision on environmental radioactivity levels).

1.1 Concepts of detection capabilities

1.1.1 Evaluation model in radiation measurements

According to the general measurement model in ionizing radiation measurement introduced in [3], the y estimate of the value of a particular physical quantity intended to be measured (the measurand, Y) is a function of the n_n net indication (net number of counts or net peak area attributed to the radionuclide of interest, for counting or spectrometry measurements, respectively) and other input quantities upon which the measurand depends, often involved in a conversion factor (denoted by w):

$$y = n_n \cdot w \quad (1)$$

For estimating the standard uncertainty associated with y , the most prevalent method is the law of propagation of uncertainty, which is the combination of standard uncertainties associated with each input quantity through a partial derivative approach. Its form in ionizing radiation measurements:

$$u(y) = \sqrt{\left(\frac{\partial y}{\partial n_n}\right)^2 \cdot u^2(n_n) + \left(\frac{\partial y}{\partial w}\right)^2 \cdot u^2(w)} = \sqrt{w^2 \cdot u^2(n_n) + n_n^2 \cdot u^2(w)} \quad (2)$$

1.1.2 Characteristic limits

Characteristic limits, such as decision threshold and detection limit, are a function of the y estimated value of the measurand and its associated $u(y)$ uncertainty which comprises both the uncertainties of the net indication ($u(n_n)$) and the conversion factor ($u(w)$). In ISO 11929:2010 [3], for the calculation of the characteristic limits the analytical approach is introduced, which is based on the propagation of uncertainties. However, new standards issued relating to the determination of characteristic limits (ISO 11929-2:2019 [4] in particular) address those matters, when calculations based on uncertainty propagation may result in inappropriate results, and alternative method, e.g. propagation of distributions should be used to provide reliable characteristic limits. Even though the analytical method is limited by several conditions, it can be still validly applicable when there is no substantial non-linearity in the measurement function and none of non-Gaussian input quantities with dominant contribution is present. Since these circumstances were met in our assessments, the corresponding concepts of characteristic limits are presented, whose interpretation is helped by the representations shown in Fig. 1.

y^* decision threshold is the value of Y , which allows the conclusion that the radionuclide assumed to generate the detected radiation is present if the measured value exceeds decision threshold ($y > y^*$):

$$y^* = k_{1-\alpha} \cdot u[y(n_n = 0)] \quad (3)$$

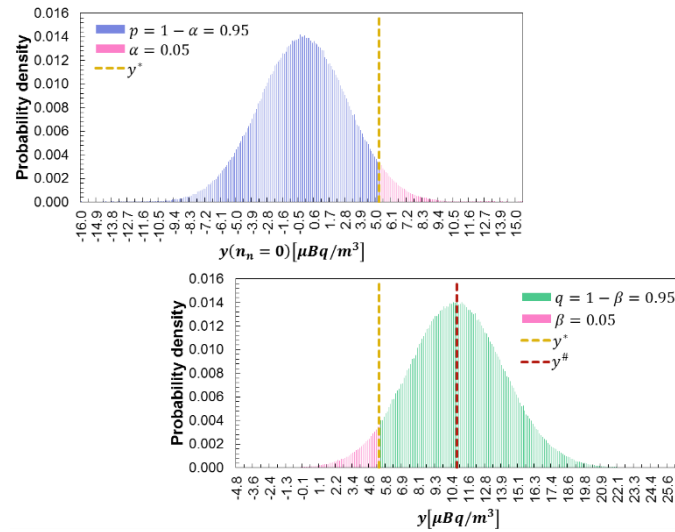
where $u[y(n_n = 0)]$ is the uncertainty estimate for the measurand when the specified quantity value is zero; $k_{1-\alpha}$ is the quantile of the standardized normal distribution for probability $p = 1 - \alpha$, with α being the probability of error of the first kind, expressing the probability of taking the wrong decision when considering the physical effect to be present even though it is absent.

The $y^\#$ detection limit is the smallest true value of the measurand for which the probability of the wrong assumption that the physical effect is absent when it is actually present (error of the second kind) does not exceed the specified probability, β . The implicit form of detection limit:

$$y^\# = y^* + k_{1-\beta} \cdot u(y^\#) \quad (4)$$

where $k_{1-\beta}$ is the quantile of the standardized normal distribution for probability $q = 1 - \beta$. The effect is observed but not quantifiable when the measured value falls between the decision threshold and detection limit ($y^* < y < y^\#$). If $y^\# < y < 4u(y)$, the effect is observed and quantified, but the result is slightly above $y^\#$ which is reflected in its relatively large $u(y)$ uncertainty. If y is unambiguously above $y^\#$ (numerically when $y > 4u(y)$), the effect is distinctly observed and quantified [5, 6].

Figure 1: Representation of the concept of y^* decision threshold and $y^\#$ detection limit



2 MATERIALS AND METHODS

2.1 Measurements of environmental samples

As part of the gamma radiation monitoring network operating at the KFKI Campus, on-line electronic dose rate meters and passive TL dosimeters provide real-time gamma dose rate and supplementary integrated gamma dose rate data, respectively. However, ambient gamma dose rate measurements did not show elevated radiation levels in the environment for any of the investigated incidents. More sensitive and energy-selective analysis of environmental samples (aerosol filters and deposition) were performed by gamma spectrometry being able to determine nuclide-specific activity concentrations of the artificial radionuclides of interest. Continuous air and deposition sampling are performed at 4 compound measurement stations (Stations 1, 2, 5, 6) following by subsequent laboratory measurements. Air flow rates at the measurement stations vary between the range of 100 and 715 m^3/day , depending on the performance of the operated air pumps. The sampling duration of air measurements ranges from 1 day- to 1 week-long interval. Sampling of wet and dry deposition (both combined and separate collection is performed, depending on the sampler type) is carried out in open-surface collectors with identical surface area of 0.2 m^2 . The routine sampling frequency for deposition measurements varies from weekly to monthly periods at the different stations. The gamma spectrometry measurements are carried out with coaxial HPGe detectors with relative efficiencies of 20...40%, in iron-shielded low-background measuring chambers. For sample measurements the routine counting time is 60 000 s, for background measurements 240 000 s typical measurement time is used.

2.2 Determination of characteristic limits of measurements

The net indication confirming the presence of the radionuclide of interest, is determined as the difference of n_g gross indication in the sample and n_0 background effect, often obtained as n_b blank indication observed with a separate measurement of a blank sample. Due to the low-level activities of investigated samples, the dead time correction was negligible, hence both t_s sample and t_b background measurement times were considered to be constant (i.e. without uncertainties) and were not included in

the conversion factor but treated separately: $y = \frac{w}{t_s} \cdot (n_g - n_0) = \frac{w}{t_s} \cdot \left(n_g - \frac{t_s}{t_b} n_b \right)$. The measurand was

the activity concentration, for gamma spectrometry w conversion factor comprised the full-energy peak efficiency (ε), the emission probability (p_γ), the sample quantity, e.g. air volume (m), the correction factors for decay during sampling (K_s), during the delay between the termination of sampling and the

start of the measurement (K_d), and during counting (K_m): $w = \frac{1}{\varepsilon \cdot p_\gamma \cdot m \cdot K_s \cdot K_d \cdot K_m}$.

2.2.1 Aspects of gamma-ray spectrum analysis

For calculation of properties of peaks that reside on a continuous background, the region-of-interest (ROI) analysis was applied assuming a linear background shape. When no peak was present at the energy region of interest and its vicinity, an estimate of the n_0 background contribution was obtained by summing the counts in the peak region with the width, x_g . When the activity value was not zero and an isolated peak (without overlapping peaks) was present at the energy of interest, the continuous background under the peak was interpolated from lower and upper spectral regions adjacent to the peak, with contents of n_1 and n_2 , respectively. According to [3], when linear background shape is assumed, the two bordering regions shall be specified with equal length, $x_1 = x_2 = x_0$. When additionally to the Compton continua full-energy peaks were also present at the energy region of interest in the blank spectrum, additional background terms related to the correction for the contribution of background peaks must have been considered. The peaked background subtraction required to account for the different sample and background measurement times ($t_s \neq t_b$), as well. The formulae used for the determination of characteristic limits in the considered variant circumstances are summarized in Table 1.

Table 1: Formulae (presented in [5, 6]) used for spectrometric measurements with background continuum and with additional presence of full-energy peaks in the background, using $k_{1-\alpha} = k_{1-\beta} = k$

Quantity	Background continuum		Background continuum + full-energy background peak ^(a)
	No peak identified	Not zero activity, isolated peak	
n_0	n_g	$\frac{x_g}{2x_0}(n_1 + n_2)$	$\frac{x_g}{2x_0}(n_1 + n_2) + \frac{t_s}{t_b} \left[n'_g - \frac{x'_g}{2x_0}(n'_1 + n'_2) \right]$
y^*	$\frac{w}{t_s} k \sqrt{2n_0}$	$\frac{w}{t_s} k \sqrt{\frac{x_g}{2x_0} \left(\frac{x_g}{2x_0} + 1 \right) (n_1 + n_2)}$	$\frac{w}{t_s} k \sqrt{\frac{x_g}{2x_0} \left(\frac{x_g}{2x_0} + 1 \right) (n_1 + n_2) + \frac{t_s}{t_b} \cdot \frac{x'_g}{2x_0} \left(\frac{t_s}{t_b} \cdot \frac{x'_g}{2x_0} - 1 \right) \cdot (n'_1 + n'_2) + \frac{t_s}{t_b} \left(\frac{t_s}{t_b} + 1 \right)}$
$y^\#$	$\frac{w}{t_s} \frac{k^2 + 2k\sqrt{2n_0}}{1 - k^2 \left(\frac{u(w)}{w} \right)^2}$	$\frac{w}{t_s} \frac{k^2 + 2k \sqrt{\frac{x_g}{2x_0} \left(\frac{x_g}{2x_0} + 1 \right) (n_1 + n_2)}}{1 - k^2 \left(\frac{u(w)}{w} \right)^2}$	$\frac{w}{t_s} \frac{k^2 + 2k \sqrt{\frac{x_g}{2x_0} \left(\frac{x_g}{2x_0} + 1 \right) (n_1 + n_2) + \frac{t_s}{t_b} \cdot \frac{x'_g}{2x_0} \left(\frac{t_s}{t_b} \cdot \frac{x'_g}{2x_0} - 1 \right) \cdot (n'_1 + n'_2) + \frac{t_s}{t_b} \left(\frac{t_s}{t_b} + 1 \right)}}{1 - k^2 \left(\frac{u(w)}{w} \right)^2}$

^(a) apostrophes denote quantities in the blank spectrum

For multi gamma-ray emitters, common characteristic limits (\bar{y}^* ; $\bar{y}^\#$) were determined based on individual characteristic limits (y_i^* ; $y_i^\#$) corresponding to the respective peaks at energies E_i ; E_j :

$$\bar{y}^* = \sqrt{1 / \sum_{i=1}^M \frac{1}{y_i^{*2}}} \quad \text{and} \quad \bar{y}^\# = \bar{y}^* + k_{1-\beta} \cdot u(\bar{y}^\#) \quad (5)$$

where $u(\bar{y}^\#)$ denotes the uncertainty corresponding to the common detection limit:

$$u(\bar{y}^\#) = \sqrt{\sum_{i=1}^M \sum_{j=1}^M v_i \cdot v_j \cdot u(y_i^\#) \cdot u(y_j^\#) \cdot r(y_i^\#, y_j^\#)} \quad , \quad \text{with weights} \quad v_i = 1 / \left[u^2(y_i^\#) \cdot \sum_{i=1}^M \frac{1}{u^2(y_i^\#)} \right]$$

corresponding to the peak at E_i , and v_j corresponding to the peak at E_j , specified on the same manner.

M denotes the number of detected peaks of the radionuclide in question; $M > 2$. The correlation coefficient is given in terms of two ratios: $r(y_i^\#, y_j^\#) = \frac{u_c(y_i^\#)}{u(y_i^\#)} \cdot \frac{u_c(y_j^\#)}{u(y_j^\#)}$, where $u_c(y_i^\#)$ and $u_c(y_j^\#)$

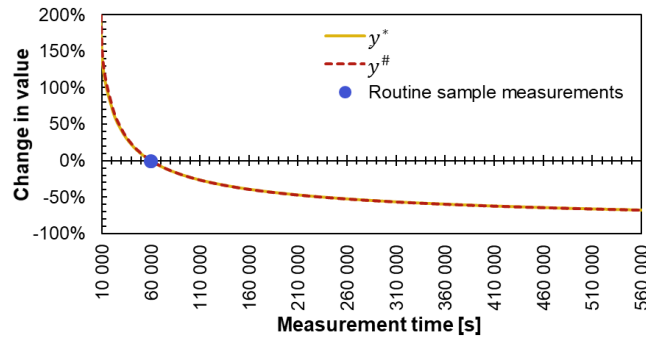
refers to the component of uncertainty originating in uncertainties of input quantities that introduce correlation. In this interpretation, combined uncertainties $u(y_i^\#)$ and $u(y_j^\#)$ can be expressed as the summation of the component introducing correlation and the component not introducing correlations [7]. Those input variables which are not introducing correlation are typically net indications and emission probabilities at different energies, whereas the efficiency, the sample quantity, the counting time and the decay correction factors are quantities that introduce correlation [6].

3 RESULTS

3.1 Effect of measurement time

y^* decision threshold and $y^\#$ detection limit are approx. inversely proportional to the square of t_s measurement time (as in Fig. 2), e.g. by quadrupling the routine measurement time, characteristic limits were reduced approx. to their half. Due to the inverse quadratic relation, it is evident that increasing the counting time reduces the characteristic limits up to a point, from which, however, no further substantial reduction can be achieved by more extension of the measurement time. Graded approach should be followed to minimize wasted effort on expansion without effective reduction. Considering some other practical aspects, measurements with extended counting times may also hinder the optimal operation as the available measurement capacities occupied for longer times. Extension is also limited by the obligation of quick data provision and the decay of short-lived radionuclides during counting.

Figure 2: Change in y^* and $y^\#$ as a function of t_s measurement time



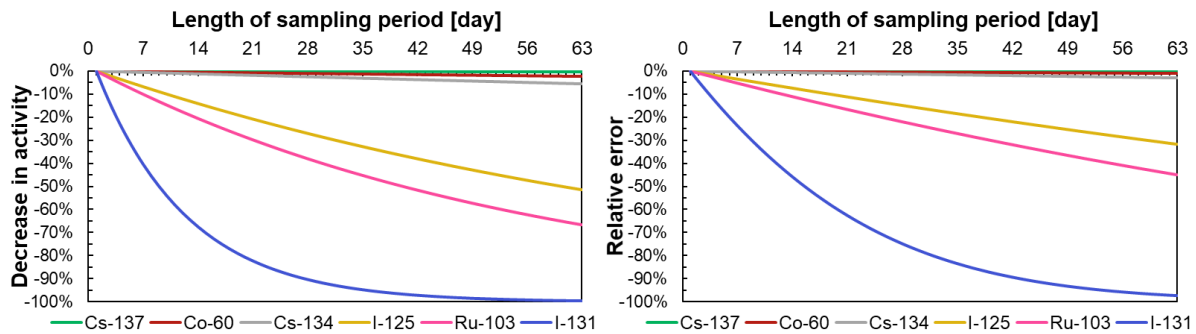
When performing a separate background measurement, counting times for both sample and background may be optimized considering the K ratio between r_n net and r_0 background count rates. The lowest relative uncertainty of r_n is reached when equation of $R = \sqrt{(K + 1)}$ is satisfied [8], where R is the ratio between t_s sample and t_b background counting times. In environmental measurements the gross count rate ($r_g = r_n + r_0$) is often similar to the background count rate ($K \approx 0$), hence for low-level activity samples it is ideal to choose same counting time for sample and background measurements. When r_0 considered to be stable in time, its uncertainty may be reduced with replicate measurements.

3.2 Effect of quantities in the conversion factor

3.2.1 Efficiency and sample volume

y^* and $y^\#$ are approx. inversely proportional to ε efficiency and m sample quantity. Increasing of efficiency to reduce characteristic limits may be feasible by using a more sensitive detector, which is however limited by technical conditions (available measuring system's characteristics) and financial constraints. Increasing the sample quantity to decrease the characteristic limits could be achieved e.g. by extending the sampling duration, which, however, may be limited by several factors, including by the necessity of urgent data provision and the effect of radioactive decay during sampling. Activity of short-lived radionuclides may decrease even below to the characteristic limits by the end of sampling due to decay. The sampling duration also affects the adequacy of correction for decay during sampling, which could only be an approximation using assumptions about the generally unknown time of appearance of the radionuclide in the sample. The recommended decay correction method is based on the assumption of continuous accumulation on sample medium since this method generates the smallest error, arising from the difference between the (unknown) true and the decay corrected activity [9]. Nevertheless, even this approach may result in significant error, in particular for short-lived radionuclides (e.g. ^{131}I), as the error increases with the extension of the sampling duration (see Fig. 3). Further systematic error will occur if the radionuclide in question was present in the sampled medium only for a short period or its concentration varied significantly during the sampling period.

Figure 3: Decrease in the activity accumulated at the very beginning of sampling due to decay (on the left); relative error arising from decay correction assuming continuous accumulation on sample medium (default approach) if accumulation happened at the very beginning of the sampling period (on the right), as a function of sampling duration, for radionuclides ^{137}Cs ($T_{1/2} = 10976$ d), ^{60}Co ($T_{1/2} = 1925.3$ d), ^{134}Cs ($T_{1/2} = 754.0$ d), ^{125}I ($T_{1/2} = 59.4$ d), ^{103}Ru ($T_{1/2} = 39.2$ d), ^{131}I ($T_{1/2} = 8.02$ d), respectively



With fixed sampling periods the sample quantity can be increased by using high-flow-rate air samplers or deposition collectors with bigger surface area, which, however, can lead to significant and costly equipment improvements. To compensate the low volume of sampled air or the small collecting area and consequent poor sensitivity, increasing of the sample quantity was accomplished by combining samples obtained over a given sampling period at the different measurement stations and measuring them collectively. By measuring all the 18 filters taken in one week (Station 1: 1 filter, changed weekly; Stations 2 and 6: 5 filters at each, changed daily on working days; Station 5: 7 filters, changed also on weekends and holidays) collectively, the sevenfold increase in air volume compared to the daily frequency and fourfold increase compared to the sampling per station resulted in a reduction of the characteristic limits to a total of twenty-eight when measuring such pooled sample. In order to achieve such a reduction (twenty-eightfold) by sole changing of measurement time, the duration of the measurement should be extended to $\sim 28^2 = 784$ times. Because in case of deposition (fallout) sampling the increase of the collecting surface is physically limited by the design of the sampling vessel, reduction of characteristic limits could be achieved by evaporating the liquid-form deposition samples taken on a monthly basis (at Stations 1,2,5) together and measuring them as a pooled sample, which resulted in a threefold increase in the sampling surface compared to one sampler evaluated per station. Monthly sampling also causes a slight improvement in the sensitivity due to the increased sample volume. As a result of the combined sample processing and measurement of monthly samples, the characteristic limits were reduced to an average of one-third compared to one sample evaluated per week. To achieve such a (threefold) reduction by sole changing of the measurement time, the duration of the measurement should be extended almost ninefold.

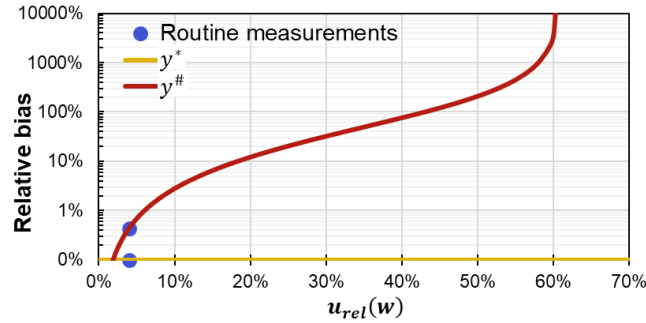
Such combination of samples should be applied if it is suspected that there is no detectable indication, when the goal is to keep the characteristic limits as low as possible. By combination of the samples, average activities can be obtained characteristic of the whole site, if more frequent monitoring of changes in activity concentrations over time or monitoring of the spatial distribution per stations is required, independent measurement of samples must be maintained. With this procedure, the data content of the measurements did not decrease significantly, the practical information content of the separate assessment per measuring station was small in our experience. This is due to the fact that the sampling sites are quite close to the on-site main potential discharge point (stack), therefore – especially in case of weak and fluctuating winds, typical of the site – separation of individual directions is not definite enough. Where the spatial distribution of activity concentrations is relevant (e.g. at Station 6, which is critical for the release of radioactive materials at the KFKI Campus as release at ground level can also be assumed in its vicinity), it is important to maintain a separate assessment for each station.

3.2.2 Uncertainties

In the analytical approach, $u(w)$ uncertainty associated to the conversion factor only influences $y^\#$ detection limit but not y^* decision threshold, as in the explicit solution for $y^\#$ a weighting function $1/[1 - k^2 \cdot u_{rel}^2(w)]$ appears (from this it follows that the explicit solution exists if $k^2 \cdot u_{rel}^2(w) < 1$).

With increase of $u_{rel}(w) = u(w)/w$ relative standard uncertainty, the detection limit is also increasing (as in Fig. 4), hence enhancement of sensitivity requires the lowest possible values for $u_{rel}(w)$. In our routine measurements $u_{rel}(w)$ was about 4%, which was dominated by the uncertainty of strongly energy-dependent efficiency and sample quantity, with contribution of about 68% and 30%, respectively. Nevertheless, the contribution of $u(w)$ to the total uncertainty $u(y)$ was significantly less than the uncertainty contribution of the net indication, so for improvement of detection capabilities effort should primarily be concentrated on the reduction of the latter (some methods described in Section 3.3.).

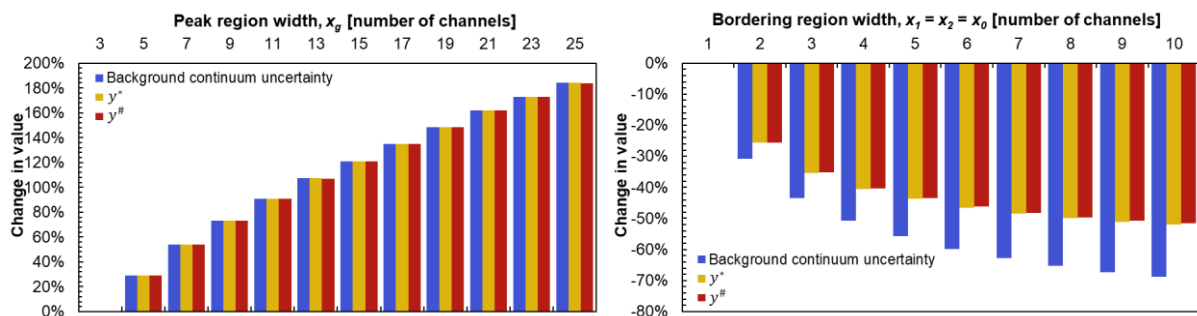
Figure 4: Relative bias corresponding to the change in y^* ; $y^\#$ as a function of $u_{rel}(w)$, for $k = 1.645$



3.3 Spectrum analysis

When a peak was not identified at the energy region of interest, there was no need to evaluate the border regions of ROI of the presumed peak to determine the continuous background, but summarizing the counts in the peak region over the width, x_g . By expansion of the peak region, the absolute uncertainty of background continuum increases due to the incremented number of counts by taking into account multiple channels, leading to elevated characteristic limits (see on the left of Fig. 5). This would suggest that the narrowest possible peak region would be ideal, but in contrast, it is important to contain the great majority of counts which pertains to the nuclide of interest. To resolve these two contradictory effects, a compromise solution must be sought when choosing the peak region width, preferably in accordance with the resolution of the measuring system. If the peak of interest was not located, the most favorable peak region width is 1.2 times the full width half maximum (FWHM), according to the recommendation of [3]. In ROI analysis, when the background continuum is determined by interpolating under the peak, the characteristic limits depend on the ratio of the number of channels in the peak and the bordering region. The uncertainty of background continuum can be made arbitrarily small by extending the bordering region (as on the right of Fig. 5). In case of a fixed peak region width (for a pronounced peak, [3] recommends to use $2.5 \times \text{FWHM}$ for the width of the peak region), as the bordering region widens (and their proportion decreases), the absolute uncertainty of the continuous background estimate and thus the value of the characteristic limits will decrease. Optimal bordering region width is $x_0 = 3 \dots 5$, when substantial reduction in the uncertainty of the background continuum and consequently in the characteristic limits is achievable but potential effect of interference with adjacent peaks is avoidable and adequacy of the approximation to linearity of the baseline is maintainable.

Figure 5: Change in y^* and $y^\#$ as a function of peak and bordering region width



Characteristic limits are increasing function of the uncertainty associated to the measurand. For multi gamma-ray emitters, the uncertainty may be decreased by determining uncertainty of the weighted mean of the activities associated with corresponding peaks. Since the characteristic limits are given in terms of the null measurement uncertainty, if uncertainty of the weighted mean is determined and common characteristic limits are formed, the common values will be lower than the individual ones corresponding to each peaks. Taken ^{60}Co and ^{134}Cs as examples (see Table 2), when common characteristic limits were formed, about 40% average reductions were achieved, compared to the individual values.

Table 2: Characteristic limit calculations for multi gamma emitters ^{60}Co and ^{134}Cs

Quantity	Individual values ^(a)				Quantity	Common values ^(a)	
	^{60}Co 1173.3 keV	^{60}Co 1332.5 keV	^{134}Cs 604.72 keV	^{134}Cs 795.86 keV		^{60}Co	^{134}Cs
y_i^* [$\mu\text{Bq}/\text{m}^3$]	5.73	5.59	5.18	6.08	\bar{y}^* [$\mu\text{Bq}/\text{m}^3$]	4.00	3.94
$y_i^\#$ [$\mu\text{Bq}/\text{m}^3$]	12.3	11.4	10.8	12.3	$\bar{y}^\#$ [$\mu\text{Bq}/\text{m}^3$]	8.41	8.17

^(a) Values given for a measurement carried out with 60 000 s counting time with a detector with 30% rel. efficiency. Pooled sample formed from aerosol filters sampled over 1 week, total air volume 4332 m³.

4 CONCLUSIONS

Effective improvement of detection capabilities can be achieved by increasing measurement time and the value of quantities included in the conversion factor (typically detection efficiency, sample quantity). Because of the inverse quadratic relation between characteristic limits and counting time, sole expansion of counting time allows a significantly smaller increase in sensitivity compared to the other parameters. By simultaneous application of different sensitivity improvement methods, several orders of magnitude improvements can be achieved in the characteristic limits. Increase of influencing quantities has several constraints both in routine and accidental environmental monitoring which necessitates optimization.

5 REFERENCES

- [1] IRSN, 2020. Information note of May 05, 2020. Retrieved 2020-05-07 from https://www.irsn.fr/EN/newsroom/News/Documents/IRSN_Information-Report_Fires-in-Ukraine-in-the-Exclusion-Zone-around-chernobyl-NPP_05052020.pdf
- [2] IRSN, 2020. Information report of July 22, 2020 "Detection of an increase in airborne radioactivity levels in Northern Europe – Update of July 22, 2020". Retrieved 2020-08-07 from https://www.irsn.fr/EN/newsroom/News/Documents/IRSN_NI-Detection-airborne-radioactivity-northern-europe_22072020.pdf
- [3] ISO 11929:2010, 2010. Determination of the characteristic limits (decision threshold, detection limit and limits of the confidence interval) for measurements of ionizing radiation – Fundamentals and application
- [4] ISO 11929-2:2019, 2019. Determination of the characteristic limits (decision threshold, detection limit and limits of the coverage interval) for measurements of ionizing radiation — Fundamentals and application — Part 2: Advanced applications
- [5] De Felice, P., Jerome, S., Petrucci, A., 2017. Practical implementation of ISO 11929:2010. Appl. Radiat. Isot., 126, 256-262. <https://doi.org/10.1016/j.apradiso.2017.02.004>
- [6] IAEA, 2017. Determination and Interpretation of Characteristic Limits for Radioactivity Measurements – Decision Threshold, Detection Limit and Limits of the Confidence Interval. Analytical Quality in Nuclear Applications Series No. 48. IAEA, Vienna. ISSN 2074-7659.
- [7] Glavič-Cindro, D., Korun, M., Vodenik, B., 2004. Correlations between the activities of a gamma-ray emitter calculated from different peaks in the spectrum. Accred. Qual. Assur., 9, 473-477. <https://doi.org/10.1007/s00769-004-0825-y>
- [8] Hurtgen, C., Jerome, S., Woods, M., 2000. Revisiting Currie – how low can you go? Appl. Radiat. Isot., 53, 45-50. [https://doi.org/10.1016/S0969-8043\(00\)00171-8](https://doi.org/10.1016/S0969-8043(00)00171-8)
- [9] Jakab, D., Pázmándi, T., Zagyvai, P., 2017. The revision of the current radioactive fallout measurements at the KFKI campus in Budapest, Hungary. 6th International Youth Conference on Energy, 21-24.06.2017, Budapest, Hungary. <https://doi.org/10.1109/IYCE.2017.8003711>